Physical atomistic kinetic Monte Carlo modeling of Fermi-level effects of species diffusing in Silicon

I. Martin-Bragado,* P. Castrillo, M. Jaraiz, R. Pinacho, J.E. Rubio, and J. Barbolla
Department of Electronics, University of Valladolid. ETSIT Campus M. Delibes, 47011 Valladolid, Spain
(Dated: October 21, 2004)

An accurate physically-based Fermi-level modeling approach, amenable to be implemented in an atomistic device-size process simulator, is reported. The atomistic kinetic Monte Carlo method is used for point and extended defects, in conjunction with a quasi-atomistic, continuum approach treatment for carrier densities. The model implements charge reactions and electric bias according to the local Fermi-level, pairing and break-up reactions between particles, clustering-related dopant deactivation and Fermi level-dependent solubility. We derive expressions that can be used as a bridge between the continuum and the atomistic frameworks. We present the implementation of two common dopants, Boron and Arsenic, using parameters that are in agreement with both ab-initio calculations and experimental results.

I. INTRODUCTION

Current microelectronic technology is facing increasingly complex phenomena related to very high-doping, reduced thermal budget (non-equilibrium conditions), and three dimensional effects. Such conditions require a deep insight into the underlying physical mechanisms in order to correctly model the material properties. In particular, high-doping concentrations demand a correct description of diffusion under extrinsic conditions.[1,2] Other charge-related issues are Fermi-level dependent solubility,[3,4] clustering-related dopant deactivation,[5] and high-damage electrical compensation.

Continuum modeling, based on solving partial differential equations (PDE) discretized by the finite element method, has been used since the 1980's, but this method is limited by the number of equations that can be solved without running into convergence instabilities. Moreover, meshing issues and dimensionality make this approach extremely complicated in 3D. The International Roadmap for Semiconductors 2003[6] establishes the "Modeling hierarchy from atomistic to continuum" among the difficult challenges that need to be solved before 2010. The atomistic kinetic Monte Carlo (kMC) method,[7] has proven to be a powerful approach that allows the inclusion of comprehensive, physically based models without significantly degrading the simulator's performance. Some semiconductor companies[8,9] and software vendors[10,11] have already started to develop simulators based on this atomistic kMC approach. Modelling Fermi level effects is one of the critical steps in developing a comprehensive kMC simulator. Here we will describe a detailed Fermi-level modeling approach specially designed to be included in this methodology, which has been implemented and tested in the atomistic kMC process simulator DADOS.[12]

We first describe in detail the basic physical models and then the particular implementation of point defects and of two representative dopants (boron and arsenic), and finally show a simulation example.

II. PHYSICAL MODELS

In this section we will introduce some concepts not explicitly present in continuum models which will allow us to adapt the formulation of Fermi-level effects in diffusion[1] to an atomistic framework.

In our simulation scheme, particles are represented atomistically, with a particular position, species, type (substitutional, interstitial) and charge. Defects are formed by such particles. Electrical equilibrium can be assumed even when particle concentrations are far from equilibrium conditions because the charge reactions are much faster than structural reactions.[13] As a consequence, the Fermi-level (e_F) is considered to be well defined and carrier concentrations are treated in a continuum fashion.

A. Concentrations of charged states

Let us consider a particle X as an example of native point defect (self interstitials, I, or vacancies, V) in silicon, which is the focus of our study. They can be in multiple charge states X^j, with $j = --, -, 0, +, ++$.

We denote by $e(j+1, j)$ the energy level associated to the charge transitions between X^{j+1} and X^j. Then, the relative concentrations are:

$$\frac{[X^j]}{[X^{j+1}]} = \frac{g^j}{g^{j+1}} \times \exp\left(\frac{e_F - e(j+1, j)}{kT}\right) \quad (1)$$

g^j being the degeneracy factor and kT the thermal energy. We assume the same degeneracy factor for all the charge states.

Our convention is to take the origin of energy levels at the valence-band edge. We can assume that the electric levels of all charged species vary with the temperature proportionally to the band gap width E_g.[14]

The concentration of neutral native point defects (I^0 or V^0) in equilibrium conditions, denoted as $[X^0]^*$, is controlled by its formation energy, $E_f(X^0)$, that is independent of e_F. From Eq. 1 one can derive the concentration

of charged states and their formation energies. The total point defect concentration as a function of e_F will be primarily determined by the charge state with lower E_f. For $e_F = e(j+1, j)$ the formation energies of X^{j+1} and X^j are the same and therefore $[X^{j+1}]^* = [X^j]^*$. Since there are no explicit assumptions of equilibrium in Eq. 1 it is still valid out of equilibrium, and then the supersaturation, defined as $S_X = [X]/[X]^*$, is the same for all the charge states:

$$[X^j]/[X^j]^* = [X^0]/[X^0]^* = S_X.$$

B. Defect diffusivities

In atomistic kMC, defect diffusivity is related to the random walk of migrating defects. The point defect migration frequency ν_m for a given charge state j of a particle X is:

$$\nu_m(X^j) = \nu_{m,0}(X^j)\exp(-E_m(X^j)/kT) \qquad (2)$$

$\nu_{m,0}$ being the migration prefactor and E_m the migration energy. Accordingly, in three dimensions,

$$D(X^j) = \lambda^2 \nu_m(X^j)/6, \qquad (3)$$

where λ is the jump distance. We have chosen λ to be equal to the second neighbors distance in the silicon lattice (0.384 nm). The transport capacity due to diffusion will be $DC(X) = \sum_j D(X^j)[X^j]$. Under equilibrium conditions the products $D(X^j)[X^j]^*$ are going to have an activation energy of $E_{\rm dif}(X^j) = E_m(X^j) + E_f(X^j)$, denoted as diffusion energy. The transport capacity will be dominated by the charge state with lower $E_{\rm dif}$.

C. Electric drift

Fig. 1 shows electric drift as a natural consequence of the local dependence of the formation energies of charged particles. Within the kMC framework, the relation between the migration frequency in the positive and negative directions along the x axis for a point defect with charge jq is

$$\frac{\nu_{m,+x}}{\nu_{m,-x}} = \exp\left(-\frac{\lambda}{kT}\frac{dE_f}{dx}\right) = \exp\left(\frac{jq\mathcal{E}_x\lambda}{kT}\right) \qquad (4)$$

where $\vec{\mathcal{E}}$ is the electric field and q is the absolute value of the electron charge. The last equality assumes constant band gap. From Eq. 4 one can derive the x-component of drift velocity to be equal to

$$v_x = \lambda(\nu_{m,+x} - \nu_{m,-x})/6$$

which, in a first order approximation, becomes the Einstein relation $v_x = jqD\mathcal{E}_x/(kT)$.

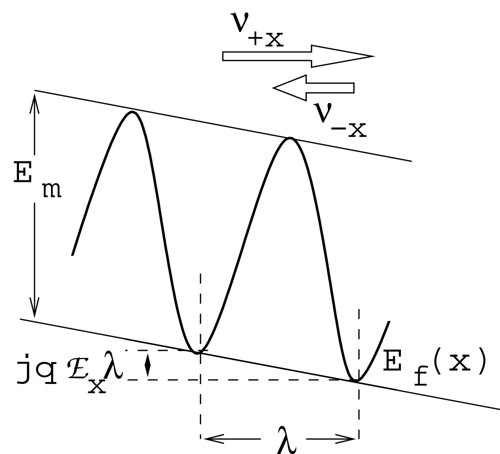

FIG. 1: Electric drift within a kMC framework (see Eq. 4).

D. Point defect reactions

Reactions between particles take place in kMC when particles are within the capture radius of each other. In our model two different reactions are implemented: pairing with impurities (A) and break up,

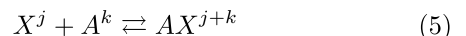

$$X^j + A^k \rightleftarrows AX^{j+k} \qquad (5)$$

conserving the charge, and reactions of equilibrium between different charge states

$$X^{j+1} + e^- \rightleftarrows X^j. \qquad (6)$$

The pairing reactions between repulsive species are forbidden. For the break up reactions, due to the charge conservation, ν_{bk} does not depend on e_F. Eq. 5 together with Eq. 6 are enough to take into account the different break up paths because we assume that the equilibrium between different charge states is instantaneous.

In the present model clusters are assumed to be neutral and only neutral particles are emitted and captured. Once the neutral particle has been emitted as a point defect, it can change its charge state according to the local Fermi level. It would be easy to implement extended defects charge states in kMC, but reliable values for physical parameters (either from calculations or experiments) would be needed.

E. Solubility

The solubility of charged species depends on e_F.[3,4] For the case of a dopant A^j, the solubility limit is given by:

$$[A^j]_{\rm max}(T) = [A^j]^{\rm intrinsic}_{\rm max}(T) \times \exp\left(j\frac{e_i - e_F}{kT}\right), \qquad (7)$$

where

$$[A^j]^{\rm intrinsic}_{\rm max} = \frac{([A^j]^{\rm extrinsic}_{\rm max})^2}{n_i} \qquad (8)$$

is the solubility in intrinsic conditions ($e_F = e_i$) and $[A^j]_{\max}^{\text{extrinsic}}$ the solubility when $[A^j]_{\max} \gg n_i$. Eq. 7 is a consequence of the fact that the formation energy of charged defects depends on e_F. In an atomistic framework expression 7 can be fulfilled by trapping and emitting only neutral particles of the type AX^0 with an emission rate independent of e_F.

F. Implementation

Physical mechanisms involving defects can be described as "interactions" (reactions between two defects when they are within a capture radius) or as "events" (performed by defects with a certain frequency). The model described here has been implemented in the atomistic simulator DADOS.[10,12,15] The main tasks that the simulator has to do, related to charged point-defects, are to maintain the right local ratio between the various charge states (Eq. 1), to compute the Fermi level (and thus the carrier concentration) and to include the electric bias effects (Eq. 4). Once the drift is properly accounted in equilibrium, $[V^0]^*$ and $[I^0]^*$ are constant even if $\nabla e_F \neq 0$. We calculate e_F within the charge neutrality approximation and using the Fermi-Dirac statistic, Band-gap narrowing[16,17] and damage induced electrical compensation.

III. POINT DEFECTS: INTERSTITIALS AND VACANCIES

A. Vacancies

The charge levels for vacancies (V^{++}, V^+, V^0, V^- and V^{--}), are well characterized,[1,18] and they are represented in Fig. 2. The dependence of the formation energies with e_F for charged vacancies using the values of table I are displayed in Fig. 3a (dashed lines). Thick dashed lines correspond to the most stable charge state (lower formation energy and higher concentration) that depends on the Fermi level. As it can be seen V^+ is a meta-stable state, i.e. it is not the minimum E_f for any value of e_F. $[V^0]^*$, that is constant with e_F, is dominant for p-doped materials and of the same order as $[V^-]^*$ for intrinsic silicon. The solid lines are the diffusion energies. E_m is different for each charged species, but we assume it does not depend on e_F.

The parameters displayed in Table I and represented in Fig. 3a has been chosen to correctly fit the vacancy transport capacity reported in Ref. 19 as well as the charge levels of Refs. 1,18. The Arrhenius plot for vacancy transport capacity with the contribution of different charge states is represented in Fig. 4a.

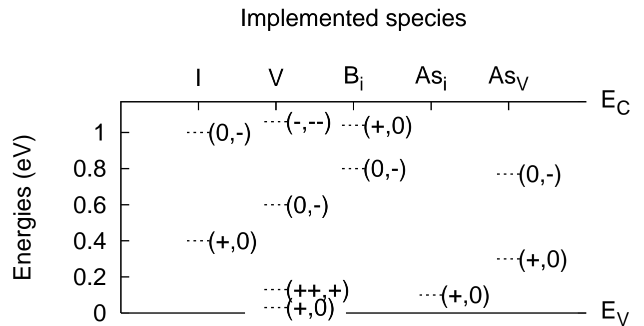

FIG. 2: Electronic levels for V, I, B_i, AsV and As_i.

B. Interstitials

The charge levels of silicon self-interstitials (I^-, I^0, I^+, I^{++}), are not conclusively established.[1,18,20] Theoretical calculations indicate that I^+ is metastable but with a very low migration energy and controls interstitial diffusion for p-doped and intrinsic materials.[20,21] However, experiments show that in intrinsic silicon, diffusion is dominated by I^0, and I^+ dominate only for $e_F < 0.4$.[1,22,23] As a simplification, and following Ref. 1, we will ignore the I^{++} state in our model, and we believe it is not necessary for continuum models as well. Therefore we will describe the interstitial using the I^+, I^0, I^- states. As we will see later (Sec. V), I^{++} presence will not change dopant diffusivity, and it only has a very small contribution to long hop distance of dopants. The values of charge levels are taken from Ref. 1.

Fig. 3b shows the formation and diffusion energies diagram that we have set for interstitials, listed in Tab. I. As commonly assumed, I^0 is the dominant state near the intrinsic conditions and I^- only has a significant contribution for heavy n-doped materials. Theoretical calculations give a migration energy for neutral interstitials of about 1 eV, so we have taken $E_m = 1.0$ eV for I^0 and we have assumed the same value for the other charge states. These parameters fit experimental data for interstitial diffusivity in intrinsic silicon.[24,25]

Figure 4b shows the Arrhenius plots for silicon self-interstitial transport capacity. The experimental points (symbols) have been extracted from Ref. 24 and 25. The lines have been calculated using the parameters displayed in table I.

IV. PAIR POINT-DEFECTS: BORON AND ARSENIC

Once the point defects, I and V, have been introduced, we will focus our study in the diffusion of dopants. Substitutional impurities are assumed to be immobile. Let us consider now the cases in which the migrating defect can be seen as the pair AX, where A is an impurity and

	I^-	I^0	I^+	V^{--}	V^-	V^0	V^+	V^{++}	B_i^-	B_i^0	B_i^+	As_i^0	As_i^+	AsV^-	AsV^0	AsV^+
$D_{m,0} \times 10^3$ (cm^2/s)	5	5	5	1	1	1	1	1	1	1	1	4.5	4.5	1	1	1
E_m (eV)	1	1	1	0.4	0.4	0.4	0.6	0.8	0.36	0.2	1.1	1.35	1.35	1.7	1.4	1.4
$e_t(T=0)$ (eV)	1		0.4	1.06	0.6		0.03	0.13	0.8		1.04		0.1	0.77		0.3
$[X^0]_0^*(\times 10^{25}$ cm$^{-3})$		690				2.6										
E_f (eV)		3.85				3.7										

TABLE I: Parameters used for charged states of silicon vacancy (V^j), silicon self-interstitial (I^j), interstitial boron (B_i^j) and vacancy and interstitial arsenic (AsV^j, As_i^j). D_0 is the diffusivity prefactor (Eq. 3), E_m the migration energy, and e_t the charge level measured from the valence band edge. For $T \neq 0$, we assume that e_t scales with band gap energy.[14] Prefactors for equilibrium concentrations and formation energies of I^0 and V^0 are also shown. Other parameters used in this work are, for boron: $D_{bk,0}(B_i^-) = 0.4\,\mathrm{cm^2s^{-1}}$, $E_b(B_i^-) = 0.1\,\mathrm{eV}$ and for arsenic: $D_{bk,0}(AsV^+) = 1 \times 10^{-3}\,\mathrm{cm^2s^{-1}}$, $E_b(AsV^+) = 1\,\mathrm{eV}$ and $D_{bk,0}(As_i^+) = 5 \times 10^{-3}\,\mathrm{cm^2s^{-1}}$, $E_b(As_i^+) = 0.1\,\mathrm{eV}$. $D_{bk,0}$ is the break-up prefactor expressed in diffusivity units ($= (\lambda^2/6)\,\nu_{bk,0}$). $D_{bk,0}$ and $E_b(T)$ can be obtained from Eqs. 11 and 12. The point defect capture volume is $2\lambda^3$.

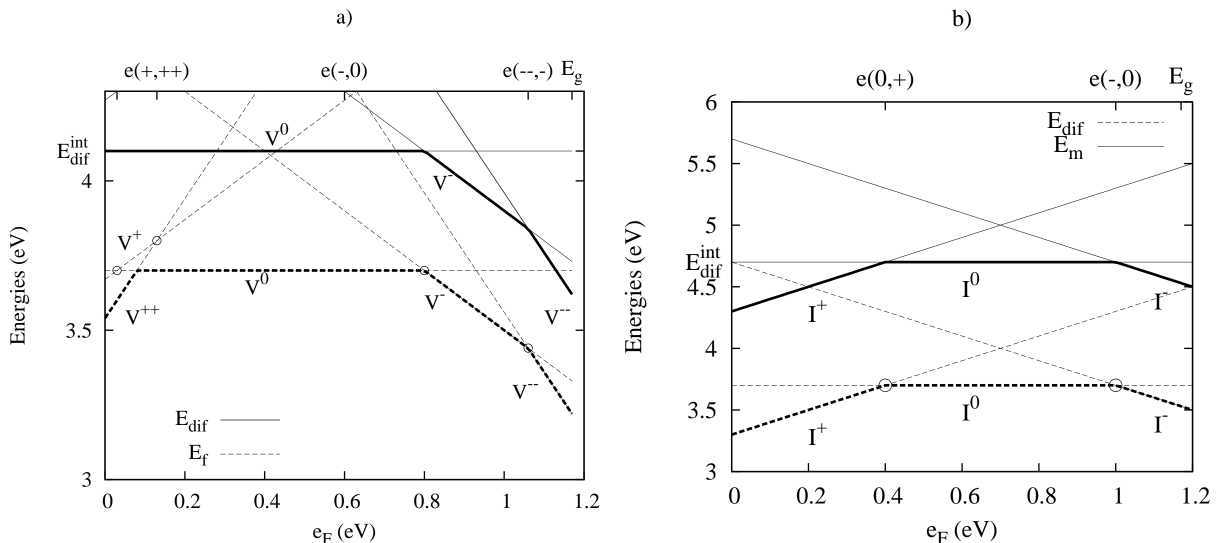

FIG. 3: Formation energies (E_f, dashed lines) and diffusion energies ($E_{dif} = E_f + E_m$, solid lines) of charged Silicon vacancy (a) and self-interstitial (b) as a function of Fermi-level (e_F) using the parameter set of Table-I. e_F is measured from the valence band edge. (Band-gap energy is $E_g = 1.17$ eV for T= 0 K). Minimum values of E_f and E_{dif} are drawn with thick lines. $E_{\rm dif}^{\rm int}$ corresponds to the diffusion energy for intrinsic Silicon ($e_F = e_i$). Open circles indicate the energy crossings corresponding to charge levels.

X is either an I or a V. We will describe first the diffusion of boron using B_i and later the case for Arsenic with AsV and As_i.

A. Boron

It is commonly accepted that B migrates mainly due to interstitial mechanism, via B_i (either as an interstitial B_i or a BI pair), rather than via V-mediated mechanism.

The known charged states of B_i are B_i^-, B_i^0 and B_i^+.[26] The three states are included in our model, although the inclusion of B_i^+ will only show up for systems far from equilibrium. The pairing, break up and charge reactions related to B_i are represented by the reactions

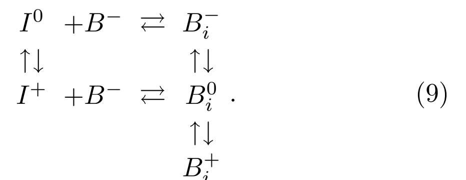

$$\begin{array}{cccc} I^0 & +B^- & \rightleftarrows & B_i^- \\ \uparrow\downarrow & & & \uparrow\downarrow \\ I^+ & +B^- & \rightleftarrows & B_i^0 \\ & & & \uparrow\downarrow \\ & & & B_i^+ \end{array} \quad . \qquad (9)$$

In the following, we assume that substitutional boron is always immobile and ionized (B^-). In Eq. 9 horizontal reactions (pairing and break-up) conserve the charge while vertical reactions establish the electrical equilibrium. The rate of the horizontal reactions will not depend on the Fermi-level. Direct break-up of B_i^+ is not included because I^{++} is not implemented. The charge level values for B_i are listed in table I and illustrated in

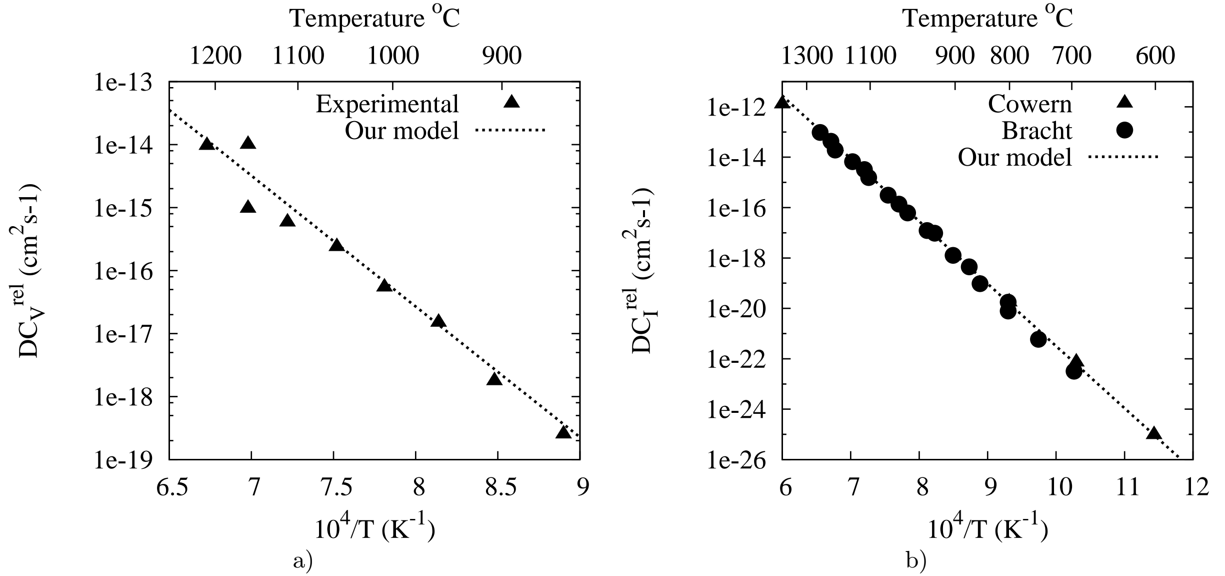

FIG. 4: Arrhenius plots for the relative transport capacity ($DC^*/[Si]$) for a) V and b) I in intrinsic conditions. The parameters are set to fit the experimental data for I[24,25] and V.[19]

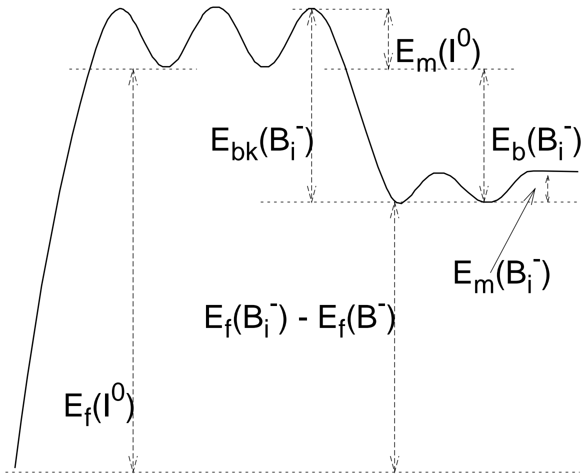

FIG. 5: Potential energy diagram showing the formation and migration energies for B_i^- and I^0, and the B_i^- binding and break up energies.

Fig. 2. These values have been measured by electrical characterization.[18,27,28]

From the first reaction in Eq. 9 the number of broken B_i^- per unit of volume and time will be $[B_i^-]\nu_{bk}(B_i^-)$ and the number of new formed $[B^-][I^0]\nu_m(I^0)v_{\mathrm{capt}}$. Consequently, in local equilibrium conditions

$$\frac{[B_i^-]}{[B^-]} = [I^0]\frac{\nu_m(I^0)}{\nu_{bk}(B_i^-)}v_{\mathrm{capt}}, \tag{10}$$

v_{capt} being the effective capture volume for pairing reaction and ν_{bk} the break-up frequency. The ratio of Eq. 10 is independent of e_F because the charges of B_i^- and B^- are the same. In contrast, $[B_i^0]/[B^-]$ and $[B_i^+]/[B^-]$ are Fermi-level dependent. The activation energies of the $[B_i^j]/[B^-]$ fractions are represented as formation energies in Fig. 6.

The activation energy for B_i^- break-up will be $E_b(B_i^-) + E_m(I^0)$ (see Fig. 5), E_b denoting the binding energy. Considering energy conservation in reactions of Eq. 9 we obtain

$$E_b(B_i^0) = E_b(B_i^-) + e_{B_i}(0,-) - e_I(+,0) \tag{11}$$

and the activation energy for B_i^0 break-up will be $E_b(B_i^0) + E_m(I^+)$. Electronic levels scale with E_g, introducing a slight T dependence in $Eb(B_i^0)$. From equilibrium conditions it can be also derived that the break-up prefactors, $\nu_{bk,0}$, have to fulfil

$$\nu_{bk,0}(B_i^0)/\nu_{bk,0}(B_i^-) = \nu_{m,0}(I^+)/\nu_{m,0}(I^0). \tag{12}$$

Boron effective diffusivity $D(B)$ is given by the sum of the contribution of all mobile species

$$D(B) = D(B_i^-)\frac{[B_i^-]}{[B^-]} + D(B_i^0)\frac{[B_i^0]}{[B^-]} + D(B_i^+)\frac{[B_i^+]}{[B^-]}. \tag{13}$$

The diffusion energy value for boron under intrinsic conditions in Fig. 6 ($E_{\mathrm{dif}}^{\mathrm{int}}$) will be similar to the activation energy of the Arrhenius plot of equilibrium boron diffusivity. The small differences can be attributed to the charge states and the modification of the charge levels with temperature. The activation energies of the terms in previous Equation (usually known as "defect-assisted diffusion energies" or just "diffusion energies", $E_{\mathrm{dif}}(B_i^j)$)

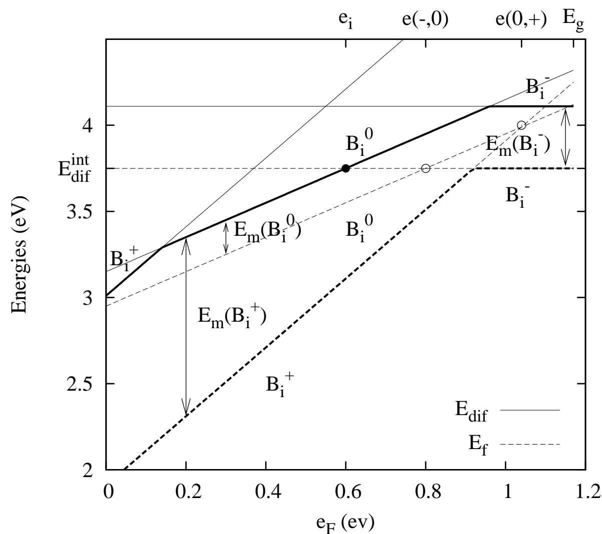

FIG. 6: Dashed lines: Energy to form a B_i^j from a B^- $(E_f(B_i^j) - E_f(B^-))$ as a function of Fermi-level using the values of Table-I. Solid lines: Activation energy of the contribution of B_i^j for the effective Boron diffusivity in equilibrium conditions, E_{dif} (see Eq. 13). Migration energies $(E_m(B_i^j))$ are the differences between solid and dashed lines. Black dot indicates the value of $E_{\rm dif}^{\rm int}$. The other notations correspond to Fig. 3.

are represented in Fig. 6. From this Figure it can be seen that B_i^0 is a meta-stable state (as $e_{B_i^+} > e_{B_i^-}$) but is the main contributor for boron diffusion in a wide range of e_F and in consequence $D(B) \propto p/n_i$ (Ref 2). According to Fig. 6 the effective migration energy of a B_i for $e_F \approx e_i$ is $E_{dif}(B_i^0) - E_f(B_i^+) \approx 0.6$ eV, in agreement with the experimental observation.[26] It is also noticeable, that one can have D_{PP} with no I^{++}. Actually, $D(B)$ does not depend on the charge states of I, but on those of B_i.

The parameters listed in Table I and used in Fig. 6 have been chosen to fit the Arrhenius plot of equilibrium boron diffusivity, $D(B)^*$ reported in Ref. 29. In particular, the binding energy of B_i^- and migration energy of B_i^0 have been taken to fit the boron diffusivity Arrhenius plot, and the migration energies for B_i^- and B_i^+ are in agreement with the picture derived from ab-initio calculations[30] and the experimental $D^*(B)$ for n type silicon.[2]

Using the Maxwell–Boltzmann approximation, Eq. 13 is usually written in continuum models as :

$$D(B) = S_I \left[D_X(B) + D_P(B)\frac{p}{n_i} + D_{PP}(B)\left(\frac{p}{n_i}\right)^2 \right], \tag{14}$$

S_I being the interstitial supersaturation, and p and n_i the hole concentration and the intrinsic concentration, respectively. The relations between the above diffusivity components $D_X(B)$, $D_P(B)$, $D_{PP}(B)$ and the microscopic parameters are therefore

$$\begin{aligned} D_X(B) &= v_{\rm capt} D(I^0)[I^0]^* \big(\nu_m(B_i^-)/\nu_{bk}(B_i^-)\big) \\ D_P(B) &= v_{\rm capt} D(I^0)[I^0]^* \big(\nu_m(B_i^0)/\nu_{bk}(B_i^-)\big) \\ &\quad \exp\big((e_{B_i}(0,-) - e_i)/kT\big) \\ D_{PP}(B) &= v_{\rm capt} D(I^0)[I^0]^* \big(\nu_m(B_i^+)/\nu_{bk}(B_i^-)\big) \\ &\quad \exp\big((e_{B_i}(0,-) + e_{B_i}(+,0) - 2e_i)/kT\big) \end{aligned} \tag{15}$$

e_i being the intrinsic level.

These expressions can be used as a bridge between the parameters of continuum simulators and those of a kMC simulator. Nevertheless, the above continuum expression assume Maxwell-Boltzmann and quasi-equilibrium conditions, which are not needed within the kMC approach. We should point out that the above terms only depends on $D(I^0)$ without dependences on I^+ or I^-. The ratios $\nu_m(B_i^j)/\nu_{bk}(B_i^-)$ mean that the diffusivity of each term can be increased by increasing the migration rate, or decreasing the break up rate, but increasing or decreasing both leaves the magnitude unchanged. The atomistic meaning is that the B diffusivity does not depend on how fast B_i moves, but on the distance traveled (long hop) by the B_i before breaking up.

For slightly doped material, the dominant diffusing interstitial is I^0, which upon interaction with substitutional boron creates a B_i^- which in turn switches to B_i^+ very quickly because B_i^+ has the lowest formation energy for these conditions. However, B_i^+ is a slow diffusant that can also switch to B_i^0, which is a fast diffusant and provides the main contribution to the overall boron diffusivity. Notice that the most frequent break up reaction is for the B_i^- charge state to fulfil microscopic reversibility of the most frequent pairing reaction.

B. Arsenic

Once boron charged states have been explained, a similar analysis can be done for arsenic, which has both vacancy and interstitial contributions, related to AsV and As_i defects, respectively. Arsenic reactions are

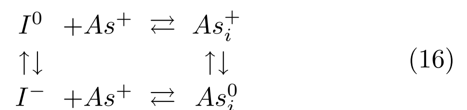

$$\begin{array}{lcl} I^0 \; +As^+ & \rightleftarrows & As_i^+ \\ \uparrow\downarrow & & \uparrow\downarrow \\ I^- \; +As^+ & \rightleftarrows & As_i^0 \end{array} \tag{16}$$

and

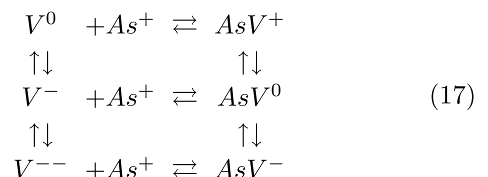

$$\begin{array}{lcl} V^0 \; +As^+ & \rightleftarrows & AsV^+ \\ \uparrow\downarrow & & \uparrow\downarrow \\ V^- \; +As^+ & \rightleftarrows & AsV^0 \\ \uparrow\downarrow & & \uparrow\downarrow \\ V^{--} \; +As^+ & \rightleftarrows & AsV^- \end{array} \tag{17}$$

where we are also assuming that As^+ is immobile and always ionized.

Arsenic diffusion will have all previously mentioned contributions

$$\begin{aligned} D(As) \;&\approx\; D(AsV^{+})\tfrac{[AsV^{+}]}{[As^{+}]} + D(As_i^{+})\tfrac{[As_i^{+}]}{[As^{+}]} \\ &+\; D(AsV^{0})\tfrac{[AsV^{0}]}{[As^{+}]} + D(As_i^{0})\tfrac{[As_i^{0}]}{[As^{+}]} \\ &+\; D(AsV^{-})\tfrac{[AsV^{-}]}{[As^{+}]} \end{aligned} \tag{18}$$

which, in continuum models is usually reduced to[31]:

$$\begin{aligned} D(As) \;&=\; [f_I S_I - (1-f_I)S_V]\times \\ &\left[D_X(As) + D_M(As)\tfrac{n}{n_i} + D_{MM}(As)\left(\tfrac{n}{n_i}\right)^2\right], \end{aligned} \tag{19}$$

f_I being the fraction of interstitial-assisted diffusion.

Notice, however, that this continuum description conveys several simplifying assumptions compared to Eq. 18. In the first place, the common assumption that D_X and D_M fit an Arrhenius plot is only true if the contributions of AsV^+ and As_i^+ have the same activation energy, and the same has to be true for the AsV^0, As_i^0 contributions. More importantly, Eq. 19 assumes that the interstitial fraction, f_I is independent of the Fermi level (i.e. the same for the three charge states), and is also independent of the temperature. These assumptions reduce the range of applicability of Eq. 19. Our parameter set for As is reported in Table I. These parameters fit the equilibrium As diffusion reported by Ref. 2. The binding energy (1.3 eV) and migration energy used for AsV^0 compares very well with ab-initio calculations.[32] The value of $e_{AsV}(0,-)$ is from Ref. 2. The activation energy of f_i is the same than the value in Ref. 33.

Figure 7 shows experimental diffusivity (symbols) reported in Ref. 2 for different concentrations and temperatures, compared with our calculated values. We have taken into account the field enhancement factor h.[1]

Figure 8 shows the good agreement between the differential equation-based model and our atomistic simulations for the case of Arsenic in-diffusion for both intrinsic and extrinsic conditions. The effect of Fermi-level is evident in the obtained box like shape profile for extrinsic diffusion. The comparison made in Figs. 7 and 8 validates the parameter translation between atomistic and continuum formulation (Eq. 15 and equivalent for As).

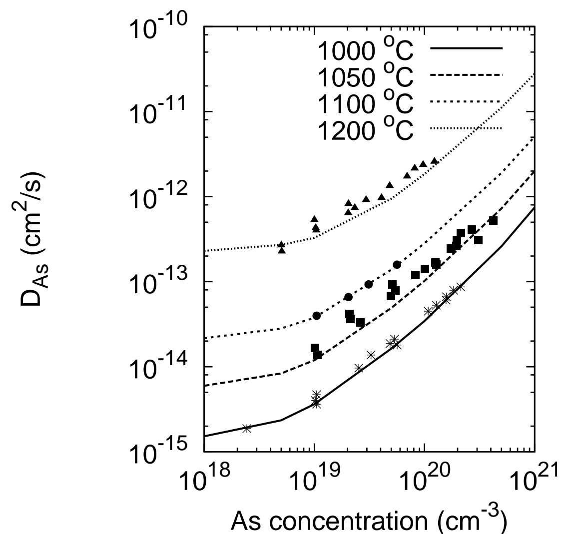

FIG. 7: Arsenic diffusion dependence on the temperature and dopant concentration. Symbols: experimental data (Ref. 2). Lines: Calculated values (see text).

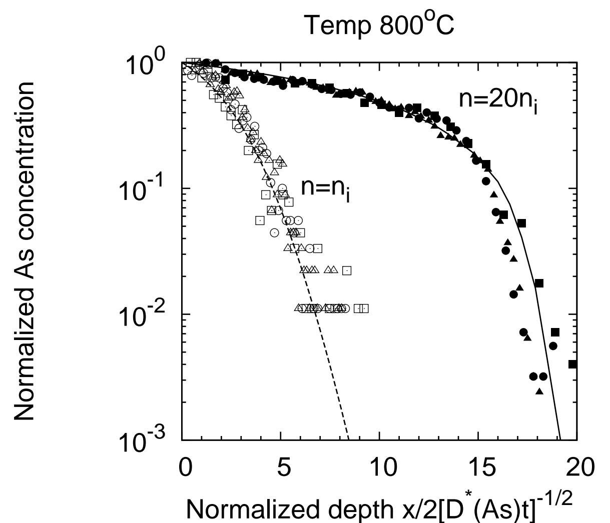

FIG. 8: Normalized Arsenic concentration profiles under intrinsic and extrinsic ($n = 20n_i$) conditions for 800° C. Lines: calculated within the continuum framework. Symbols: kMC simulations (squares: 1.4×10^4 s, circles: 4.6×10^4 s, triangles: 10^5 s). In order to do an even comparison, Maxwell-Boltzmann statistics has been used in our simulation.

V. DOPANT LONG HOPS INVOLVING SEVERAL CHARGE STATES

In systems where diffusion proceeds via an intermediate migrating species the shape of the diffusion profiles of dopants can be substantially different, even though the standard deviations of the profiles are the same.[34,35] This is because the shape is controlled by the value of the long hop distance, Λ, (distance traveled by a point defect pair before breaking up), which is given by[35,36]

$$\Lambda = \lambda\sqrt{\frac{1}{6}\frac{\nu_m}{\nu_{bk}}}, \tag{20}$$

taking for ν_m and ν_{bk} their average charge states. In the above mentioned case of a B_i, Eq. 20 becomes

$$\Lambda = \lambda\sqrt{\frac{1}{6}\frac{\nu_m(B_i^-)[B_i^-] + \nu_m(B_i^0)[B_i^0] + \nu_m(B_i^+)[B_i^+]}{\nu_{bk}(B_i^-)[B_i^-] + \nu_{bk}(B_i^0)[B_i^0]}}$$

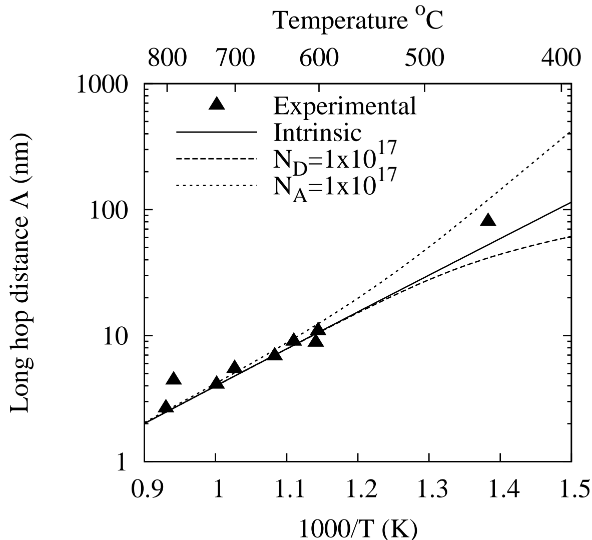

FIG. 9: Arrhenius plot for B_i long hop distance (Λ). Lines: values calculated using our parameter set for intrinsic, n-doped and p-doped silicon. Symbols: experimental values in quasi-intrinsic conditions.[25,34,37]

which using Eq. 10 and equivalent can be written as

$$\Lambda = \lambda \sqrt{\frac{1}{6} \frac{\nu_m(B_i^-)\frac{[B_i^-]}{[B^-]} + \nu_m(B_i^0)\frac{[B_i^0]}{[B^-]} + \nu_m(B_i^+)\frac{[B_i^+]}{[B^-]}}{v_{capt}(\nu_m(I^0)[I^0] + \nu_m(I^+)[I^+])}} \tag{21}$$

and, finally using Eqs. 3 and 13

$$\begin{aligned} \Lambda &= \lambda \sqrt{\frac{D(B)}{6v_{\rm capt}\{D(I^0)[I^0]+D(I^+)[I^+]\}}} \\ &\approx \lambda \sqrt{\frac{D^*(B)}{6v_{\rm capt}DC^*(I)}}. \end{aligned}$$

The last equality assumes that the I^- contribution is negligible. $DC^*(I)$ is the equilibrium transport capacity of interstitials. With the values we are using, $\Lambda \propto \sqrt{p/n_i}$ for $e_F \simeq e_i$.

The temperature dependence of Λ for boron, using the parameters of table I is displayed in Fig. 9, both for intrinsic and doped silicon, and compared with experimental values for intrinsic materials.[34,37]

It is interesting to note that the concentrations of the different charge states of interstitials (namely I^+ and I^-) do not directly affect boron diffusivity (see equations 13 and 15). This could suggest that, as a simplifying approximation, one can neglect the presence of I^- and I^+. However, Eq. 21 shows that, by doing so, an incorrectly large Λ value could be obtained for extrinsic materials. In fact, the magnitude of $D(B)$ is governed by the $\nu_m(B_i^j)[B_i^j]/[B^-]$ terms, but how Gaussian the diffusion profile is, depends also on the $\nu_m(I^j)[I^j]$ terms.

VI. AN EXAMPLE: A COMPLEX SCENARIO

One of the reasons for developing the detailed modelling of charge effects presented in this work is that, in the complex processing scenarios which are now common place in advanced semiconductor manufacturing, the dominant mechanisms may not be apparent or, even worse, one can be misled by intuition.

As an example, Fig. 10 corresponds to a typical 10 keV, 5×10^{14} cm^{-2} As^+ implant onto a 2×10^{18} cm^{-3} uniformly B doped substrate followed by a 10 min., 750 °C anneal. This apparently simple experiment involves a number of different mechanisms and the simulation will only be predictive against changes in the processing conditions if each and every mechanism is correctly implemented. Namely, the simulator accumulates damage (taking into account the dose rate and implant temperature) and correctly predicts the amorphization of the top 75 nm layer and the electrical deactivation of the dopants in the damaged regions. Recrystallization occurs during the simulation of the temperature ramp up. In agreement with experimental evidence the simulated recrystallization front partially sweeps B and As, and deposits electrically active dopants up to a maximum level, depositing the rest as small defect-dopant clusters. In the simulation, the EOR interstitial clusters evolve to {311} defects and, eventually to dislocation loops. The presence of the loops lowers dramatically the interstitial supersaturation and slows down transient enhanced diffusion (TED). During TED, B is depleted from the junction and piles up as it enters the N side. However, it is interesting to remark that this apparent electric drift effect was actually associated to a net flux of the neutral B_i^0, maybe against simple intuition. Namely, the gradient of e_F produces a gradient of $[B_i^0]/[B^-]$ and, in consequence, a diffusion flux of B_i^0 toward the N-region that tends to homogenize $[B_i^0]$. Boron pile-up in the As-rich region is a result of the lower value of D(B) in N-type materials (See Eq. 14). The Figure shows experimental results[38] as symbols, and simulation results as lines. The agreement is good, taking into account the number of mechanisms involved in the atomistic simulation as described above.[39]

VII. CONCLUSIONS

In this work an accurate, physically-based atomistic modeling of Fermi-level effects of species diffusing in Silicon has been presented. This model takes into account the charge reactions and electric bias dependency with Fermi-level, pairing and break-up reactions between particles, clustering dopant activation and deactivation and the Fermi-level dependent solubility. It also includes degenerate Fermi-Dirac statistics, band-gap narrowing and damage-induced electrical compensation.

The presented model, in particular Eq. 15, establishes a bridge between atomistic kMC and continuum approaches for Fermi-level dependent diffusivity. From

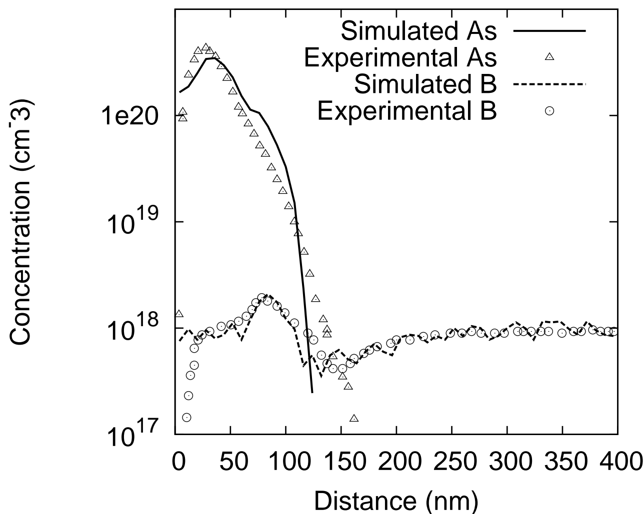

FIG. 10: Dopant redistribution in a PN junction. Initially boron has a homogeneous concentration close to 2×10^{18} cm^{-3} (P region). The N^+ region has been implanted (As, 10 keV, 5×10^{14} cm^{-2}) and, subsequently, the sample has been annealed by 10 min. at 750°C (Experimental data from Ref. 38).

the practical point of view it has the added value of being amenable to implementation in device size atomistic kMC process simulators.[10] These atomistic simulators are expected to play an increasingly relevant role in the forthcoming years[6] due to their ability to directly incorporate ab-initio parameters and complex mechanisms.

VIII. ACKNOWLEDGMENTS

This work has been partially supported by the Spanish Government under project BFM 2001-2250 and by the Castilla y Leon Regional Government under project VA-010/02. The authors would like to thank C. Mok for proof reading the paper.

* Electronic address: `ignacio.martin@tel.uva.es`

1 P. M. Fahey, P. B. Griffin, and J. D. Plummer, Reviews of Modern Physics **61**, 289 (1989).
2 R. B. Fair, *Impurity doping processes in Silicon* (North-Holland, 1981).
3 J. E. Northrup and S. B. Zhang, Phys. Rev. B. **47**, R6791 (1993).
4 C. G. V. de Walle, D. B. Laks, G. F. Neumark, and S. T. Pantelides, Phys. Rev. B **47**, 9425 (1993).
5 L. Pelaz, G. H. Gilmer, V. C. Venezia, H.-J. Gossmann, M. Jaraiz, and J. Barbolla, App. Phys. Lett. **74**, 2017 (1999).
6 Several, *International technology roadmap for semiconductors*, http://public.itrs.net (2003).
7 M. Jaraiz, G. H. Gilmer, J. M. Poate, and T. D. de la Rubia, Appl. Phys. Lett. **68**, 409 (1996).
8 M. Hane, T. Ikezawa, K. Takeuchi, and G. H. Gilmer, in *IEDM 2001 proceedings* (2001), p. 38.4.1.
9 M. Yu, R. Huang, X. Zhang, Y. Wang, and H. Oka, in *IEICE Transactions of Electronics*, edited by H. Iwai, SISPAD (Electronic Society, 2003), vol. E86-C, pp. 295–300.
10 V. Moroz, N. Strecker, and M. Jaraiz, in *Proceedings of the 32nd European Solid state device research Conference 2002*, edited by G. Baccarani, E. Gnani, and M. Rudan (2002), pp. 299–302.
11 B. Sahli, C. Muller, E. Alonso, and W. Fichtner, in *The 11th Symposium on Nano Device Technology* (SNDT, 2004).
12 M. Jaraiz, P. Castrillo, R. Pinacho, I. Martin-Bragado, and J. Barbolla, in *Simulation of Semiconductor Processes and Devices 2001*, edited by D. Tsoukalas and C. Tsamis (2001), pp. 10–17.
13 C. Rafferty, in *Internat. Conf. on Simulation of Semicond. Processes and Devices (SISPAD 1997)* (1997).
14 S. M. Sze, *Physics of semiconductor devices* (John Wiley & Sons, Inc., New York, 1981), 2nd ed.
15 Synopsys, *Taurus reference Manual*, Mountain View, CA,USA, 2003rd ed. (2003).
16 S. C. Jain and D. J. Roulston, Solid State Electronics **34**, 453 (1991).
17 C. Persson, U. Lindefelt, and B. E. Sernelius, J. App. Phys. **86**, 4419 (1999).
18 G. D. Watkins, Materials in Semiconductor Processing **3**, 227 (2000).
19 A. Giese, H. Bracht, N. A. Stolwijk, and D. Baither, Materials Science and Engineering B **71**, 160 (2000).
20 J. Zhu, Computational Materials Science **12**, 309 (1998).
21 W. A. Harrison, Phys. Rev. B **57**, 9727 (1998).
22 K. P. Chik, Radiation Effects **4**, 33 (1970).
23 H. Bracht and A. R. Schachtrup, in *Defects and diffusion in silicon processing* (Materials Research Society, 1997), vol. 469, pp. 25–36.
24 H. Bracht, N. A. Stolwijk, and H. Mehrer, Phys. Rev. B **52**, 16542 (1995).
25 N. E. B. Cowern, G. Mannino, P. A. Stolk, F. RoozeBoom, H. Huizing, J. van Berkum, F. Cristiano, A. Claverie, and M. Jaraiz, Materials Science in Semiconductor Processing **2**, 369 (1999).
26 G. D. Watkins, Phys. Rev. B **12**, 5824 (1975).
27 R. D. Harris, J. L. Newton, and G. D. Watkins, Phys. Rev. Lett. **48**, 1271 (1982).
28 R. D. Harris, J. L. Newton, and G. D. Watkins, Phys. Rev. B **36**, 1094 (1987).
29 Y. M. Haddara, B. T. Folmer, M. E. Law, and T. Buyuk-

limanli, Appl. Phys. Lett. **77**, 1976 (2000).

[30] W. Windl, M. M. Bunea, R. Stumpf, S. T. Dunham, and M. P. Masquelier, Phys. Rev. Lett. **83**, 4345 (1999).

[31] *"SUPREM-IV.GS. Two Dimensional Process Simulation for Silicon and Gallium Arsenide"*, Standford University (1993).

[32] M. Ramamoorthy and S. T. Pantelides, Phys. Rev. Lett. **76**, 4753 (1996).

[33] S. Matsumoto, Y. Ishikawa, and T. Niimi, J. Appl. Phys. **54**, 5049 (1983).

[34] N. E. B. Cowern, G. F. A. van de Walle, D. J. Gravesteijn, and C. J. Vriezema, Phys. Rev. Lett. **67**, 212 (1991).

[35] N. E. B. Cowern, K. T. F. Janssen, G. F. A. van de Walle, and D. J. Gravesteijn, Phys. Rev. Lett. **65**, 2434 (1990).

[36] R. Pinacho, P. Castrillo, M. Jaraiz, I. Martin-Bragado, and J. Barbolla, J. Appl. Phys. **92**, 1582 (2002).

[37] N. E. B. Cowern, G. F. A. van de Walle, P. C. Zalm, and D. J. Oostra, Phys. Rev. Lett. **69**, 116 (1992).

[38] H. S. Chao, P. B. Griffin, and J. D. Plummer, in *Mat. Res. Soc. Symp. Proc. Vol 469* (Mat. Res. Soc., 1997), vol. 469, pp. 347–352.

[39] The As profile discrepancy is mostly due to the as implanted profile generated by the binary collision program used.[12]